High-fidelity modelling of a six-turbine tidal array in the Shetlands

P. Ouro[1], A. MacLeod[2], H. Mullings[1], P. Stansby[1], T. Stallard[1]

Abstract—**To-date a very small number of tidal stream turbine arrays have been deployed at tidal stream sites, each comprising a handful of devices that aim to demonstrate the viability of this technology before its up-scaling, i.e. installing 'large', multi-row arrays. During array layout design the predictability of tidal flows allows to determine the preferred location of the turbines within a consent area, but this can become a complex task due to the presence of irregular bathymetry and interactions occurring between individual turbines. Here three- and six-turbine arrays are simulated using the high-resolution Digital Offshore Farms Simulator (DOFAS) tool, based on large-eddy simulation and actuator line method, to investigate the effect of bathymetric effects on wake recovery and performance. Thereafter, predominant flood and ebb tides are simulated, with results showing that both flow and bathymetry asymmetry leads to different wake characteristics and thus interaction between turbine wakes in different rows. A relevant finding is that, during ebb tide, the downhill bathymetry generates an adverse pressure gradient that delays wake recovery, affecting the performance of further turbines located downstream. This is observed in the simulation of another row of three turbines at 20 diameters downstream, where wake effects from the first row are expected to negligible and their performance is even lower than the obtained when the second row is spacing at 12 diameters downstream. For these multi-row configurations, during the flood tide, the favourable pressure gradient leads to the turbines to have nearly the same thrust and power coefficient, essentially indicating that momentum in the wake is fully recovered even for the 12 diameters intra-row spacing in which some wake effects from upstream turbines would be expected. Finally, wake profiles from the large-eddy simulations are compared with an analytical Gaussian wake model, showing very good agreement with the wakes of individual turbines except when multiple wakes merge or bathymetry delays wake recovery. Large eddy simulations also capture a change of turbulent flow onto the second row of turbines, the interaction of wakes with bathymetry impacting the wake position within the water depth and the merging between adjacent wakes, highlighting their essential role in the future design of tidal arrays.**

Index Terms—**Tidal turbine arrays, Large-eddy simulation, Bathymetry, Wakes, tidal turbines, turbulence**

I. Introduction

THE development of the tidal stream energy industry is at the crucial stage of proving the reliability of the technology (both bottom-fixed and floating) and to reduce the levelised cost of energy to become competitive with technologies such as floating offshore wind. Advantages of tidal turbines are their high power density [1] compared to other renewable energy technologies, relatively smaller turbine rotor size compared to wind turbines which can ease manufacturing and logistics of future > 2 MW devices, amongst others [2].

During recent years, there have been a number of projects developed in the UK and Europe focus on fostering the tidal stream industry, including the €45.5M TIGER project that aimed to deploy tidal turbines at several sites in UK/French waters in the English channel and help to advance the maturity of the technology across different levels, and the EU-funded enFAIT project that aims to demonstrate the development, operation and decommissioning of the world's largest tidal array (six turbines), over a five-year period (2017-2022), to prove a cost reduction pathway for tidal energy and that it can be cost competitive with other forms of renewable energy. Advancement in the tidal stream energy sector are also supported by the UK's Government Contracts for Difference Scheme (CfD). The 2022 CfD Round 4 awarded support for the deployment of 41 MW tidal stream turbine capacity in UK waters with a subsidised cost of £178 per MW, mainly awarded to the Meygen Phase 2 with 28 MW (about 14 turbines) and Eday 1 and 2 projects with an expected capacity of 7.2 MW from Orbital Marine Power's floating technology. The successful delivery of these projects will help to gain technology maturity whilst decreasing costs [3].

Prior to a turbine array deployment, the tidal resource needs to be characterised in order to evaluate key hydrodynamic aspects such as flow direction during ebb and flow tides, vertical distribution of velocities and turbulence intensity, turbulence lengthscale, etc. Measurement of such characteristics typically requires the use of bed- or vessel-mounted Acoustic Doppler Current Profiler (ADCPs) which can be costly, time-consuming or even difficult to retrieve from the site [4]–[6]. Recent developments using drone measurements enable surface velocities to be obtained [7], albeit with the inherent difficulty to estimate any flow characteristic below the free-surface. Alternatively, computational tools can be applied, with differing fidelity available. Two-dimensional shallow-water models are capable of estimating the depth-averaged velocity and flow direction with good accuracy [8], [9] unless there

This project was partly supported by the EPSRC Impact Acceleration Account [EP/R51150X/1] project "Optimisation of the world's largest tidal turbine array using a virtual offshore farm simulator" hosted at Cardiff University (UK) in collaboration with the Offshore Renewable Energy Catapult (UK). The authors would like to acknowledge the support of the Supercomputing Wales project, which is partially funded by the European Regional Development Fund (ERDF) via the Welsh Government.'

Affiliations: (1) School of Engineering, The University of Manchester, UK. (2) Offshore Renewable Energy Catapult, UK.

Digital Object Identifier:
https://doi.org/10.36688/ewtec-2023-442

are recirculating wakes when accuracy is compromised [10], [11] and helping to inform layout optimisation [12], whilst have limited capabilities to resolve the turbulence in the flow as they are normally based on the Unsteady Reynolds-Averaged Navier-Stokes (URANS) equations that time-average the flow for small scales. These models have also been shown to predict deflected wakes for non-yawed turbines [9], [13]. Further progress has been done with expanding the shallow-water framework to three-dimensional models, e.g. Delft3D [8] or Telemac-3D [11], [14], allowing to partly account for the vertical variability of the flow that is introduced by bathymetry changes. These models can be considered as resource modelling tools as they have proven useful to quantify whether a site is deemed suitable depending on its power density [15]. However, turbine-induced effects and loading on the device cannot be estimated from shallow waters, as common turbine rotor representation is as a source point, or capture a transient turbulent onset flow.

At array scale, tidal stream turbines operate in close proximity one another and the siting of individual turbines within arrays is dependent on multiple factors including the bathymetry at the site, flow direction and available water depth, amongst other logistics and economical criteria [12], [16]. When deployed in multiple rows, turbines are likely to operate in the wake of upstream devices, thus subjected to an unsteady velocity field of high turbulence and lower velocity magnitude, mostly depending on the distance between turbines. Array layout tools that capture these complex phenomena are invaluable to ensure that turbines capture the largest kinetic energy from the flow so as to maximise their performance whilst diminishing fatigue loads. Such tools need to be able to resolve the turbulence of the approach flow, turbulent wake shed by the turbines and, ideally, interference from surface waves and uneven bathymetry [2]. High-fidelity models based on Large-Eddy Simulation (LES) have the capability to resolve the mentioned flow scales adopting actuator line or disc methods to simplify turbine representation, as fully wall-resolved simulations of multiple turbines is impractical [17]. Despite being computationally more expensive than RANS models [18] (mid-fidelity models), LES-based models increase the accuracy to resolve the turbine wakes and thus provide reliable estimates of the interaction between turbines and how the site morphological characteristics can drive the local flow [19].

This paper presents the application of an in-house LES code, DOFAS, for the layout assessment of a small tidal array deployed in the Shetlands (United Kingdom) focusing on the interaction between the two rows of three turbines comprising the arrays as well as the effect of the highly irregular bathymetry (large downhill/uphill slope) that this site exhibits.

II. Site and tidal turbine array description

The considered tidal stream turbines are the two-bladed horizontal axis turbine designs from NOVA Innovation Ltd with 100 kW rated capacity that were deployed at Bluemull Sound in between the islands of Yell and Unst in Shetlands, United Kingdom [13]. Each NOVA turbine has a rotor diameter (D) of 9.0 m, attached to a 10 m long hub whose diameter is equal to 1.0 m. The hub-height above the seabed is 9.0 m and the approximate mean water depth at the turbines is 28 m, i.e. there is a clearance of 14.5 m between the blades top tip and water surface. These turbines are currently in operation at the site as part of the Enabling Future Arrays in Tidal (EnFAIT), an EU Horizon 2020 flagship tidal energy project. The spatial location and hub height of the turbines referenced to the minimum bathymetry elevation (deemed as $z = 0$) is presented in Table I.

The flood and ebb tide flow data were estimated adopting the vertical distribution presented in Macleod et al. [13] with an estimated bulk depth-averaged velocity (U_0) of 1.85 m/s. The ADCP tidal rose shows the flood tide at a deviation of 28° from the North direction and the ebb tide being 8° from the South direction [13]. Seabed bathymetry from the site is shown in Fig. 1, obtained from the freely-accessible EMODnet website.

TABLE I
COORDINATES OF THE TURBINE SIMULATED FOR THE DIFFERENT ARRAY CONFIGURATIONS AND ELEVATION ABOVE THE MINIMUM BATHYMETRY POINT CONSIDERED AS $z = 0$.

Turbine	Northing	Easting	z at ebb	z at flood
T_1	6730895	610077	25.76	26.12
T_2	6730908	610113	28.51	27.88
T_3	6730933	610051	25.24	25.56
T_4, X_s=12D	6731010	610065	25.55	25.77
T_5, X_s=12D	6731010	610095	26.41	26.12
T_6, X_s=12D	6731010	610125	28.23	28.01
T_4, X_s=20D	6731100	610065	24.77	25.04
T_5, X_s=20D	6731100	610095	25.37	25.79
T_6, X_s=20D	6731100	610125	25.72	26.62

A close top-view from the bathymetry distribution where turbines are deployed is presented in Fig. 1 depicting the flood and ebb flow directions and computational domains used for each of them, and location of the bed-mounted ADCP and three turbines belonging to the first row of turbines deployed (T_1 to T_3). This site is characterised by a large horizontal curvature both to the North and South to the array location with pronounced slopes, e.g. the maximum depth of 50 m is reached about 400 m from the headland on its the West side of the site, closest to the shoreline, whilst the turbine array is located in shallower water with turbine hub depths of 25–30 m. Thus, a highly three-dimensional oncoming flow could be expected during both tidal cycles.

In this study, three arrays are investigated, namely a single-row array that represents the first three turbines to be deployed, and two-row arrays adopting two streamwise spacing of approx. 12D and 20D, respectively. The turbine T_1 is considered as the reference device when deploying the other turbines in the computational domain.

Due to data confidentiality, neither the hydrodynamic characteristics of the blades were available, nor thrust and power coefficients. Thus, the blade geometry and performance data from the TGL turbine

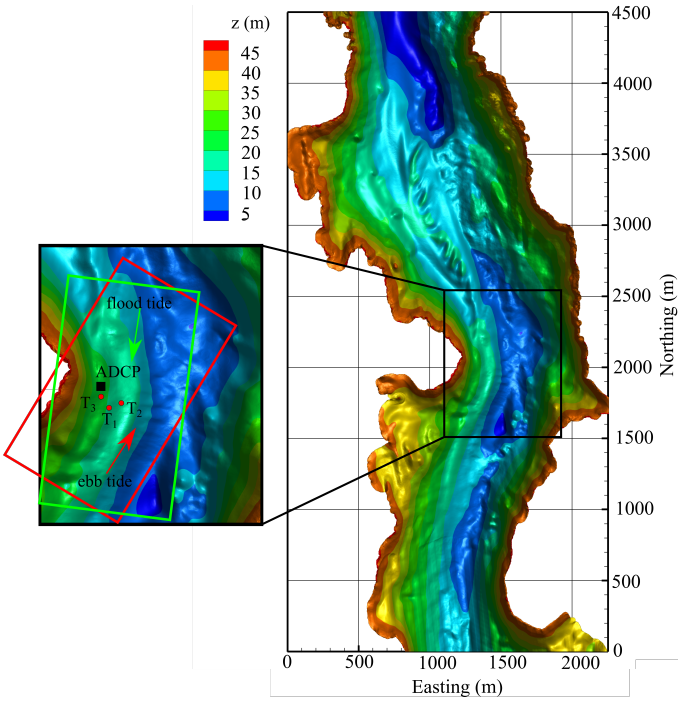

Fig. 1. Bathymetry at Bluemull Sound (Shetlands, UK) where the enFAIT tidal array is deployed. The close top-view to the array location shows the seabed mounted ADCP and first three turbines and provides the flow direction attained during each tidal phase with the computational domains for the ebb (red rectangle) and flood (green rectangle) flow directions.

modelled in the ReDAPT project by Ahmed et al. [20] with the geometry and hydrofoil properties described by Scarlett et al. [21] are adopted herein, with the chord and turbine radius scaled by a factor of 0.5 given the difference in turbine diameter with the modelled devices. Given this adapted design, the modelled turbines have a rated power output of approx. 100 kW and assumed to reach peak power coefficient at a tip-speed ratio of approx. 4.5 according to blade-element momentum [21], yielding a rotational speed (Ω) of 2.0 rad/s according to the reference velocity value considered.

III. DOFAS: Digital Offshore Farms Simulator

The high-fidelity simulations are carried out using DOFAS [22], an in-house large-eddy simulation open-source code that is built upon Hydro3D [23]–[25], which is fully parallelised with the Message Passing Interface (MPI) protocol [26], [27], including bespoke features to simulate rotating wind and tidal stream turbines, namely an efficient Actuator Line Model (ALM) and Actuator Disc Model (ADM). DOFAS adopts the Large-Eddy Simulation (LES) turbulence closure in which the most energetic and largest flow structures are explicitly resolved whilst the small scales are modelled using a sub-grid scale method, considering the filter size to be that of the numerical grid [28]. The governing equations are the spatially filtered Navier-Stokes equations for incompressible viscous flows, that read

$$\nabla \cdot \boldsymbol{u} = 0 \tag{1}$$

$$\frac{\partial \boldsymbol{u}}{\partial t} = -\frac{1}{\rho}\nabla p + \nabla(\boldsymbol{u}\cdot\nabla\boldsymbol{u}) + (\nu+\nu_t)\nabla^2\boldsymbol{u} + f_i \tag{2}$$

Here $\boldsymbol{u} = (u, v, w)^T$ is the velocity vector, the coordinates vector is $\boldsymbol{x} = (x, y, z)^T$, ρ denotes the fluid density, p is the relative pressure, t is time, ν is the kinematic viscosity of the fluid, and f_i is a source term that takes into account the ALM forces as well as those from the direct-forcing immersed boundary method adopted to represent the turbine nacelles and bathymetry. The term ν_t represents the turbulent viscosity introduced by the sub-grid scale model, in the current work this is the Wall-Adapting Local Eddy-viscosity (WALE) from Nicoud and Ducros [29] as it does not require an explicit treatment of ν_t when in proximity to walls or immersed boundary bodies.

In the resolution of the blade forces from the ALM, the non-divergence free velocities are interpolated into the blade markers using an anisotropic kernel region that varies the area of influence with the actual chord length at every Lagrangian marker. Based on the relative velocity and angle of attack and tabulated lift and drag coefficients, the resulting lift and drag forces from every marker is computed. The latter forces are projected into the Cartesian grid using the previous interpolation functions [22], [30].

Rectangular Cartesian meshes are used in DOFAS to discretise the computational domain as this allows to use numerical schemes such as central differences that enable computationally fast calculations of the fluxes while keeping a high accuracy to resolve the flow features. A fully explicit time integration scheme is adopted, with a predictor-corrector fractional step method in which a low-storage three-step Runge-Kutta scheme is used to obtain the non divergence free velocity field and an algebraic multi-grid method is implemented to resolve the Poisson pressure equation. The latter provides the pseudo pressure field that is used to correct the velocity field so it fulfils the divergence free condition and the final pressure values are also updated according to these velocities.

DOFAS has been previously validated and applied in several studies regarding tidal stream turbine flows, reporting new findings about impact of layout in infinitely long arrays [30], influence of row spacing on turbine rotor loading [22], instantaneous unsteady loading and wake recovery when a turbine is deployed over irregular bathymetry [31], or even to assess Blade Element Momentum models to estimate turbine loading from LES-computed velocity fields [32].

A. Computational setup

The computational domain is set to cover a length of 600 m by 300 m, in the horizontal plane whilst vertically is 46 m deep as it corresponds t the maximum water depth at the site (see Fig. 1. Three scenarios are considered: (i) flat bathymetry case with a constant water depth of 46 m; (ii) ebb tide (South to North) with flow incidence of 28 deg, and (iii) flood tide

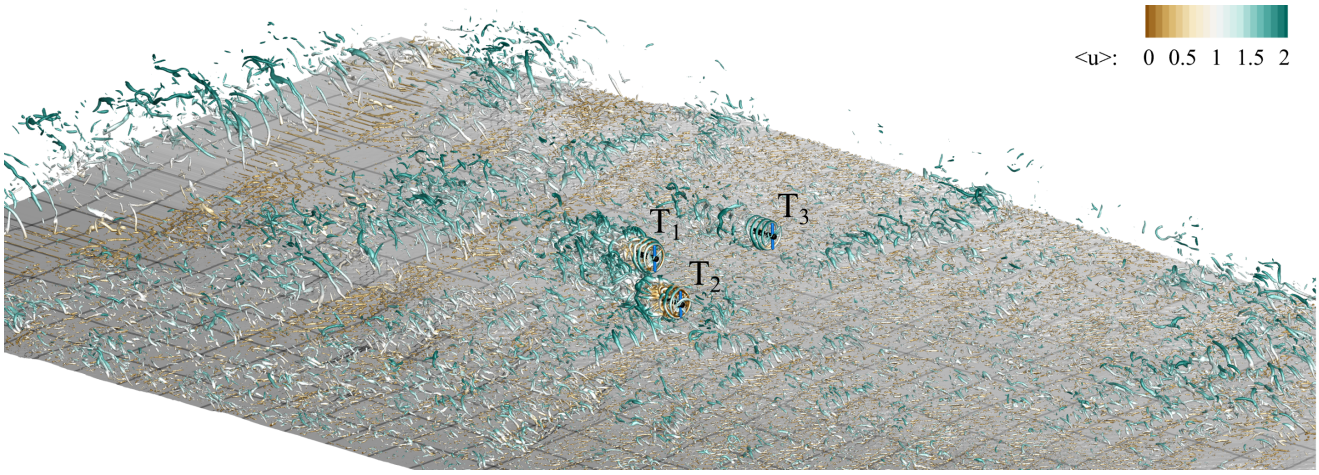

Fig. 2. Instantaneous flow field generated during the flood tide when a single row of three turbines is deployed. Vortical structures are represented using Q-criterion iso-surfaces.

(North to South) with an incidence angle of 8 degrees. For the latter two cases, the domain is rotated to be aligned with the dominant flow direction as it allows to use standard inflow-outflow boundary conditions and avoids potential numerical issues at the side boundaries that would originate from using periodic lateral conditions with a non-periodic bathymetry. Turbine T_1 is adopted as the rotation centre for generating the ebb and flood domains with secondary rows aligned with each flow direction.

A uniform grid resolution of 0.25 m is adopted throughout the domain, leading to a total number of 540 million cells. The time step is fixed at 0.06 s which equates to an averaged CFL value of approx. 0.8. Simulations are run on Supercomputing Wales facilities, using 225 CPUs running for 144 hours with an equivalent computational expense of approx. 32,500 CPU hours, which outlines the computational efficiency of DOFAS for the simulation of real-scale tidal arrays. The total simulation time was approx. 30 minutes (1,800 s). First-order statistics are collected after discarding the first 500 s, and second-order moments start to be collected after another 500 s.

At the inlet, the velocity profiles measured by the ADCP and presented in [13] are imposed with U_0 = 2.0 m/s, without inflow turbulence due to the lack of data about turbulence intensity and lengthscales. At the outlet, a Neumann boundary condition is imposed and in the lateral direction slip conditions are adopted. Buffer regions extending over 50 m in the streamwise direction are generated at the inlet and outlet of the domain in order to ease the boundary conditions convergence, e.g. avoiding large velocity gradients due to changes in bathymetry in cells nearby the domain limits. A shear-free rigid lid is set at the free-surface layer. The bathymetry is represented using a direct-forcing immersed boundary method as it has been validated in previous studies with irregular bathymetry [31]. In the flat-bed cases, a hydraulically smooth wall-function is adopted at the bottom boundary.

IV. Results

The presence of a wide spectrum of turbulent structures in the simulated tidal flow is presented in Fig. 2 for the single row case during the flood tide. Here turbulent structures are represented using Q-criterion iso-surfaces, which depict the tip vortex breakdown behind each of the three turbines. In this case, turbine T_2 undergoes a more unsteady approach flow due to bed roughness whilst T_3 operates in more less turbulent conditions.

A. Time-averaged velocity field

The time-averaged flow field, wake evolution behind T_1 and hydrodynamic coefficients of the three different tidal turbine array layouts (single row and two rows with increasing streamwise spacing) operating at the Bluemull Sound is presented in this Section.

Figure 3 presents the time-averaged streamwise velocity field at the hub-height of turbine T_1 for the three tidal turbine arrays during the ebb tide flow direction (see Fig. 1), in which the headland is seen to the upper side of the turbine T_3 whilst the deeper part of the site is on the southern region. The velocity field in Fig. 3 depicts the unevenly distributed flow field due to the bathymetry. In the single row case, the wake from turbines T_2 and T_3 are seen to extend for a long distance downstream whilst that of T_1 interacts with the bathymetry about $10D$ downstream. When a second row is deployed, the interaction between the upstream row is clear despite their spacing. With X_s = $12D$, the downstream turbine T_5 operates in the bypass flow of T_1 and T_3 whilst T_6 is highly affected by the wake of T_2. Increasing the row spacing decreases the wake effect on the secondary row. The wakes downstream of T_4 to T_6 appear to merge shortly downstream, creating an area of large velocity deficit.

The results obtained for the flood tide are presented in Fig. 4 for the three different turbine array layouts. In this case, the approach flow is not as disturbed by the headland as in during the ebb tide but there is a notable reductions in flow speed for those turbines near the headland due to their shallower conditions.

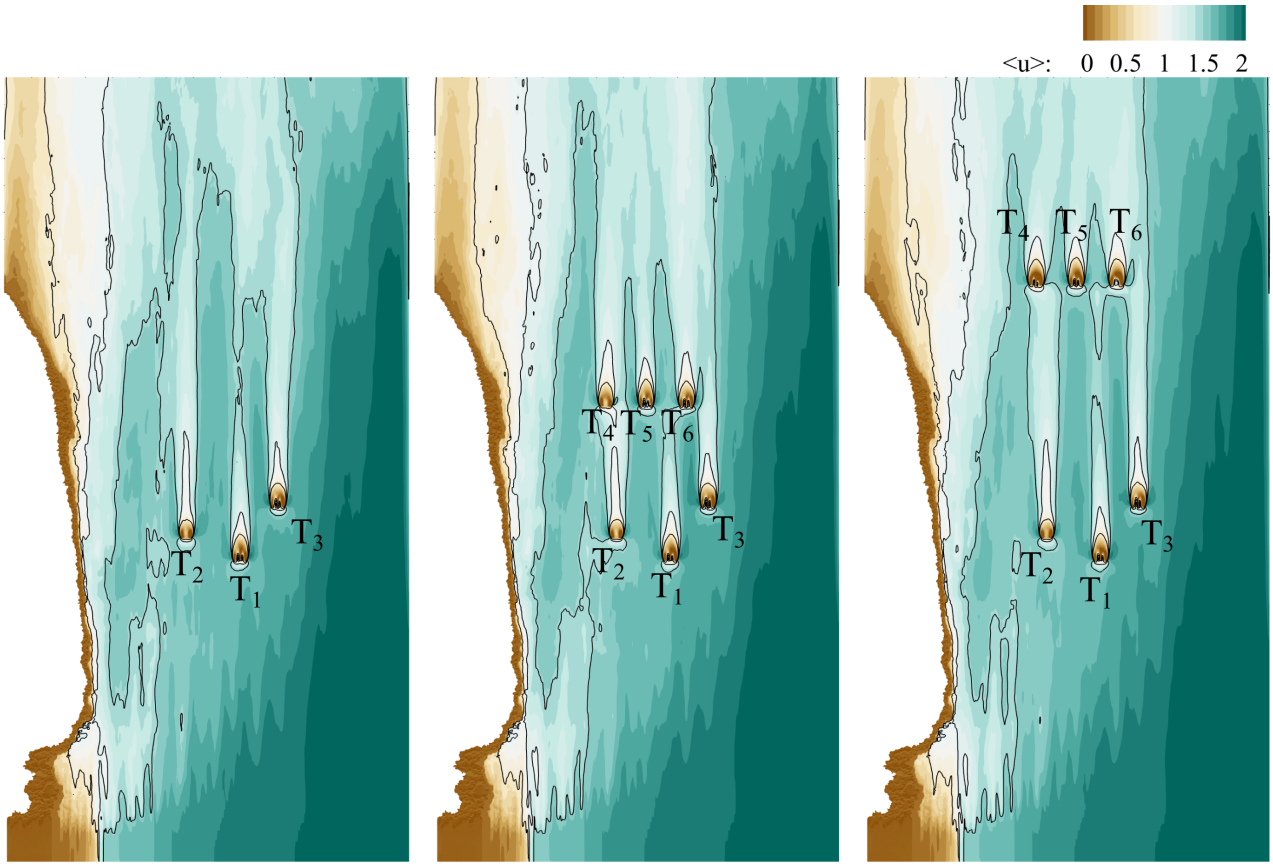

Fig. 3. Contours of time-averaged streamwise velocity at T_1 hub height for the three tidal turbine arrays simulated, namely single row (left), two rows with 12D spacing (centre), and two rows with 20D spacing (right), during the ebb tide. Flow is from bottom to top.

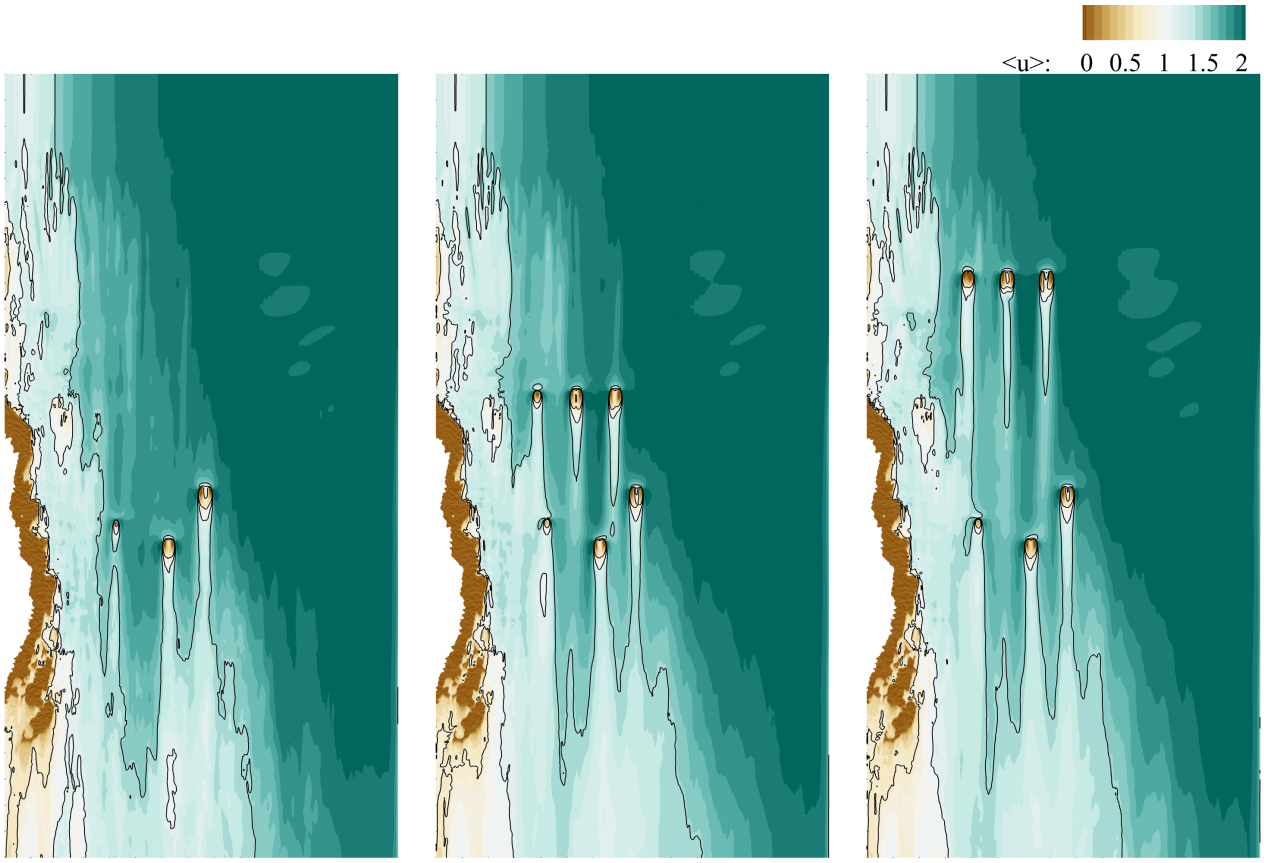

Fig. 4. Contours of time-averaged streamwise velocity at T_1 hub height for the three tidal turbine arrays simulated, namely single row (left), two rows with 12D spacing (centre), and two rows with 20D spacing (right), during the flood tide. Flow is from top to bottom. Turbine labling is analogous to that in Fig. 3.

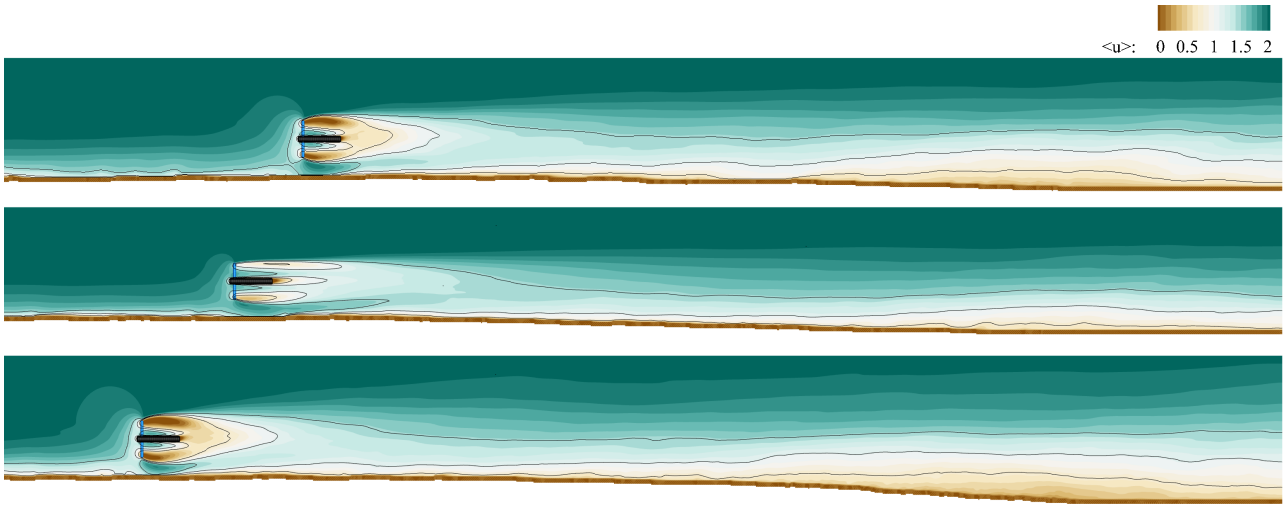

Fig. 5. Contours of time-averaged streamwise velocity over a vertical plane through the hub height of T_3 (top), T_2 (middle) and T_1 (bottom) for the case with only one row deployed. Flow direction corresponds to ebb tide. Flow is from left to right.

In the southern region of the channel, higher velocities are observed.

For the three-turbine array, the wakes from the different devices are distinct and these remain quite similar when the other row (in this case upstream) of turbines is deployed, especially for T_1 and T_2. When the second row of turbines is operating, they generate three distinct wakes as the local approach velocity is slightly different due to the bathymetry effect.

In all cases, independently to the flow direction, a larger wake from the array as a whole is observed downstream of the devices with a marked area of velocity deficit extending over a wider region compared to that extended of the individual wakes. Such results are essential when designing multi-row arrays as another hypothetical row of three turbines located to the south of the first row (considering flood tide, Fig. 4) would operate in a highly turbulent and low-momentum region, hence modification of performance should be expected relative to devices on a single row only.

This site in Bluemull Sound has marked changes of seabed slope. During the ebb tide, the flow developed downstream of the first row experiences an adverse pressure gradient due to the downhill slope. This is observed to reduce the wake recovery rate as seen in Fig. 5 with contours of mean streamwise velocity over vertical planes through the centre of the wakes of the first row turbines without a second row operating. The change in bathymetry is noticeable after about 20 diameters downstream, especially behind T_2 which is nearer to the centre of the channel and in deeper water conditions. The vertical expansion of the wake is seen to almost reach the free-surface near the end of the computational domain where the depth has increased to 32 m for this flow direction. When comparing the vertical distribution of velocities upstream of the turbines and far downstream, it is seen that there is a large velocity deficit even after 20–30 diameters downstream due to the downhill slope in the seabed.

Conversely, during flood tide, the uphill slope between the second row of turbines and devices T_1 to T_3 acts as a favourable pressure gradient that increases the wake recovery rate. This can be observed in Fig. 4 when comparing the array with two rows and X_s = $20D$, for which the velocity approaching the first row is higher during the flood tide than the ebb tide.

B. *Wake profiles*

Analytical wake models have been shown to predict to reasonable accuracy the far-wake behind tidal turbines when operating in flat bed [33], [34], i.e. in zero-pressure gradient flows, whilst some modifications to take into account positive and adverse pressure gradients have been proposed in Shamsoddin et al. [35] for wind turbines in presence of hills.

To evaluate the complex three-dimensional behaviour of the tidal turbine wakes, the wake of T_1 is depth-averaged over the rotor height and compared with an analytical wake model from Stallard et al. [33] that was obtained for a depth of $1.67D$ and assuming a Gaussian distribution of the velocity deficit (ΔU = $U - U_0$), which reads:

$$\frac{\Delta U}{\Delta U_{max}} = exp\left(-ln(2)\frac{y^2}{y_{1/2}^2}\right) \tag{3}$$

$$\frac{\Delta U_{max}}{U_0} = 0.864\left(\frac{x}{D}\right)^{-1/2} - 0.126 \tag{4}$$

$$\frac{y_{1/2}}{D/2} = 0.412\left(\frac{x}{D}\right)^{1/2} + 0.5 \tag{5}$$

where $y_{1/2}$ denotes the wake half-width, ΔU_{max} is the maximum velocity deficit and U_0 is the bulk velocity of the flow.

The prediction of the Gaussian wake model (Eqs. 3 – 5) is compared to the current LES results in Fig. 6 for T_1 in configurations with a single row with a flat-bed and considering ebb and flood tide directions. In absence of an irregular bathymetry, the wake model captures the wake evolution both in maximum velocity deficit and lateral spread from x/D = 4 onwards, whilst there is a minor underestimation in the profile closes to the turbine. During the ebb tide, the theoretical wake

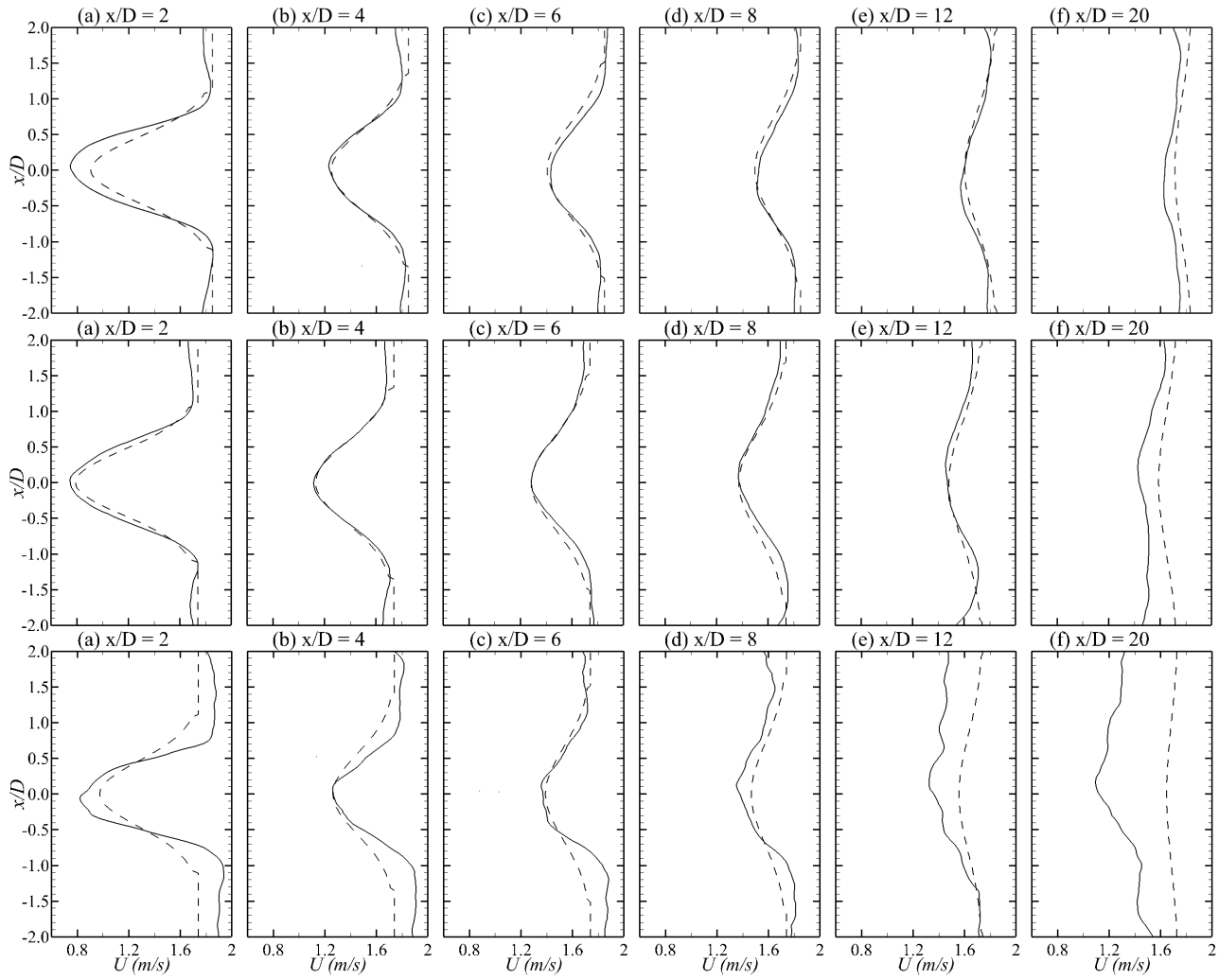

Fig. 6. Transverse profiles of streamwise velocity depth-averaged over the rotor height for turbine T_1 obtained from the LES (solid line) and Gaussian wake model (dashed line). Results for the flat (top), ebb tide (middle) and flood tide (bottom) cases.

model agrees in the central region of the wake at all location until x/D = 20, when there is a slight deviation likely due to the merging of the wake of turbine T_1 with that of T_2 and also the vertical expansion due to the increasing depth that slows down the flow (Fig. 5.

However, during the flood tide there is a worse agreement between the analytical model and the LES-computed wake, which is predicted to be narrower shortly behind the turbine and for $x/D > 10$ there is a larger velocity deficit in the simulations mostly due to bathymetry effects.

To further assess the ability of the wake model to capture the wake behaviour simulated, Fig. 7 presents the downstream evolution of the characteristic velocity scale (ΔU_{max}, Eq. 3) for the single row simulated with flat bed and bathymetry cases during ebb and flood tides. As seen in the transverse profiles, the theoretical model captures the decay of maximum velocity deficit along the wake up to about 12–24 diameters downstream, when it start to deviate from the LES due to external factors to the own turbine wake as is the bathymetry. For the flood tide case, the pressure gradient induced by the uneven bathymetry limits the capability of the wake model to predict the wake. In Fig. 6, comparing the profiles at x/D = 12 and 20, it is seen that there is no wake recovery during this distance.

C. Array performance

Performance and both steady and unsteady loading on each turbine varies during the tidal cycle due to curvature in the flow direction, bathymetry effects both accounting for wall-induced turbulence and non-zero slope, and wake effects due to turbines operating upstream.

The thrust and power coefficients computed in simulations with bathymetry during flood and ebb tides for the three arrays considered are presented in Fig. 8 together with results from a flat-bed simulation, in which T_7, T_8 and T_9 refer to the second row turbines T_4 to T_6 with X_s = 12D. During ebb tide, turbines T_1 to T_3 achieve values of mean thrust and power coefficients of 0.616 and 0.242 with the device in the centre attaining higher values due to blockage effects [22], which are slightly lower than in the flat-bed case with mean C_x and C_p of 0.640 and 0.28, respectively. These values are increased during flood tide to C_x = 0.648 and C_p = 0.328, i.e. whilst thrust load increases about 5% the turbines produce approx. 34% more. This uneven power production during the tidal phases is

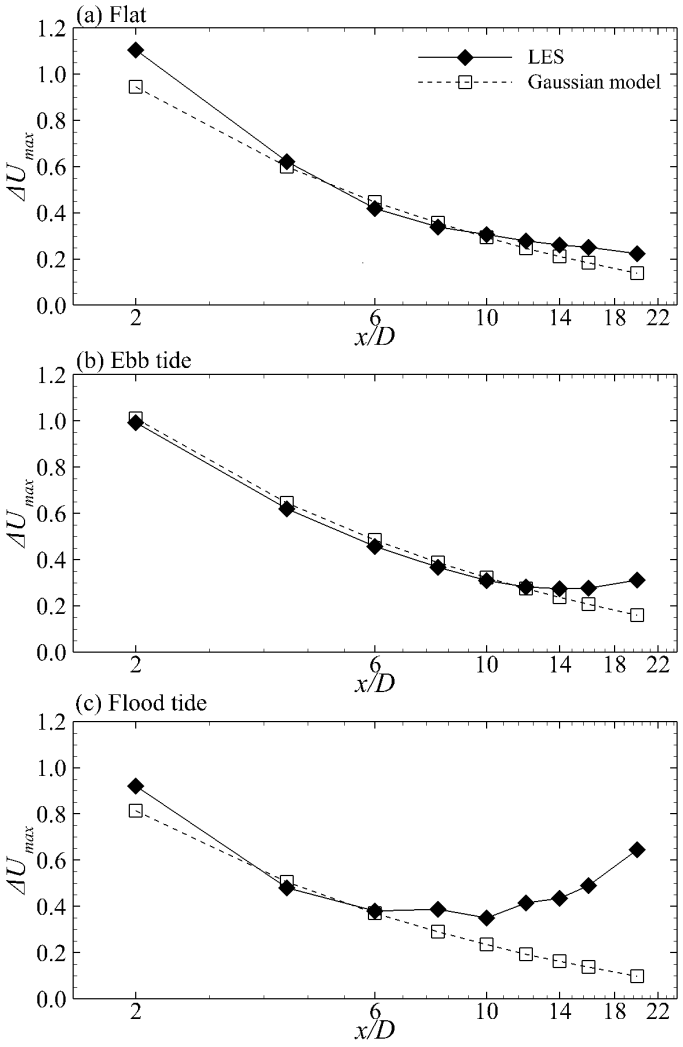

Fig. 7. Comparison of the LES-computed and analytical wake model (Eqs. 3 – 5) predictions of the maximum velocity deficit (ΔU_{max}) over the wakes downstream of turbine T_1 for the flat-bed and bathymetry cases with ebb and flow tides.

linked to the positive effect of bathymetry in the flood tide which accelerates onset velocity, e.g. observed in the bypass flow of transverse profiles in Fig. 6 at x/D = 2 for the ebb and flood tides.

Considering the two-row arrays, increasing the row spacing from X_s = 12D to 20D does not provide a noticeable improvement to the energy yield of the array irrespective to the flow direction or bathymetry condition. Considering the intra-row spacing of X_s = 20D, the hydrodynamic coefficients for turbines T_7 to T_9 indicate the wake effects are reduced (see Fig. 3) and they attain coefficients of C_x = 0.617 and C_p = 0.232 during ebb tide, with higher values of C_x = 0.647 and C_p = 0.336 during flood tide.

For the row spacing of X_s = 20D, a similar performance is observed during the flood tide, with mean C_x = 0.650 and C_p = 0.332 for T_4 to T_6 as the flow approaches these second-row devices mostly undisturbed (and are upstream of T_1 to T_3). However, during ebb tide the performance of turbines T_7 to T_9 drop to a mean value of C_p = 0.181 whilst the thrust coefficient reduced to 0.573, as a result of the effect from the uneven bathymetry.

V. Conclusions

This paper presents high-fidelity large-eddy simulations of an operative tidal stream turbine array using the state-of-the-art DOFAS (Digital Offshore Farms Simulator). Ebb and flood tides have been simulated due to the large flow asymmetry at the site due to the uneven bathymetry, and the impact of these bathymetric effects on wake dynamics and turbine loading and performance has been assessed in comparison to simulations with flat bottom and analytical wake models.

The results presented outline that bathymetry effects can play a larger role than turbine wake effects for closely-spaced turbine rows. The former can directly impact wake recovery positively if the flow moves towards a uphill-like seabed (favourable pressure gradient) but negatively if water depth increases when approaching turbines (adverse pressure gradient). In both cases, rough bathymetry acts as a source of turbulence that can aid the wake recovery.

Time-averaged wakes, depth-averaged across the rotor height, showed a good agreement with predictions from an analytical wake model based on a Gaussian wake shape until downstream distances of 12–14 diameters. This theoretical model failed to capture the wakes during the flood tide as the simulated wake is narrower at its onset and expands asymmetrically in the lateral direction further downstream.

This study demonstrates the applicability of high-fidelity, turbulence resolving simulations to fully understand the hydrodynamics of tidal stream turbine arrays at complex sites and hence inform turbine- and array-design. To improve confidence in the use of numerical tools, and to select tools of appropriate fidelity for turbine design, array siting and yield prediction, future work will be required to validate predictions for unsteady onset flows, turbine wakes and turbine performance relative to measurements obtained from full-scale conditions.

References

[1] P. Ouro, P. Dené, P. Garcia-Novo, T. Stallard, Y. Kyozuda, and P. Stansby, "Power density capacity of tidal stream turbine arrays with horizontal and vertical axis turbines," *Journal of Ocean Engineering and Marine Energy*, vol. 9, pp. 203–218, 2023.

[2] P. Stansby and P. Ouro, "Modelling marine turbine arrays in tidal flows," *Journal of Hydraulic Research*, vol. 60, pp. 187–204, 2022.

[3] D. Coles, A. Angeloudis, D. Greaves, G. Hastie, M. Lewis, L. Mackie, J. McNaughton, J. Miles, S. Neill, M. Piggott, D. Risch, B. Scott, C. Sparling, T. Stallard, P. Thies, S. Walker, D. White, R. Willden, and B. Williamson, "A review of the UK and British Channel Islands practical tidal stream energy resource," *Proceedings of the Royal Society A: Mathematical, Physical and Engineering Sciences*, vol. 477, p. 20210469, 2021.

[4] I. A. Milne, R. N. Sharma, R. G. J. Flay, and S. Bickerton, "Characteristics of the turbulence in the flow at a tidal stream power site," *Philosophical Transactions of the Royal Society A: Mathematical, Physical and Engineering Sciences*, vol. 371, p. 20120196, 2013.

[5] I. Fairley, P. Evans, C. Wooldridge, M. Willis, and I. Masters, "Evaluation of tidal stream resource in a potential array area via direct measurements," *Renewable Energy*, vol. 57, pp. 70–78, 2013.

[6] P. Garcia Novo and Y. Kyozuka, "Field measurement and numerical study of tidal current turbulence intensity in the Kobe Strait of the Goto Islands, Nagasaki Prefecture," *Journal of Marine Science and Technology (Japan)*, vol. 22, pp. 335–350, 2018.

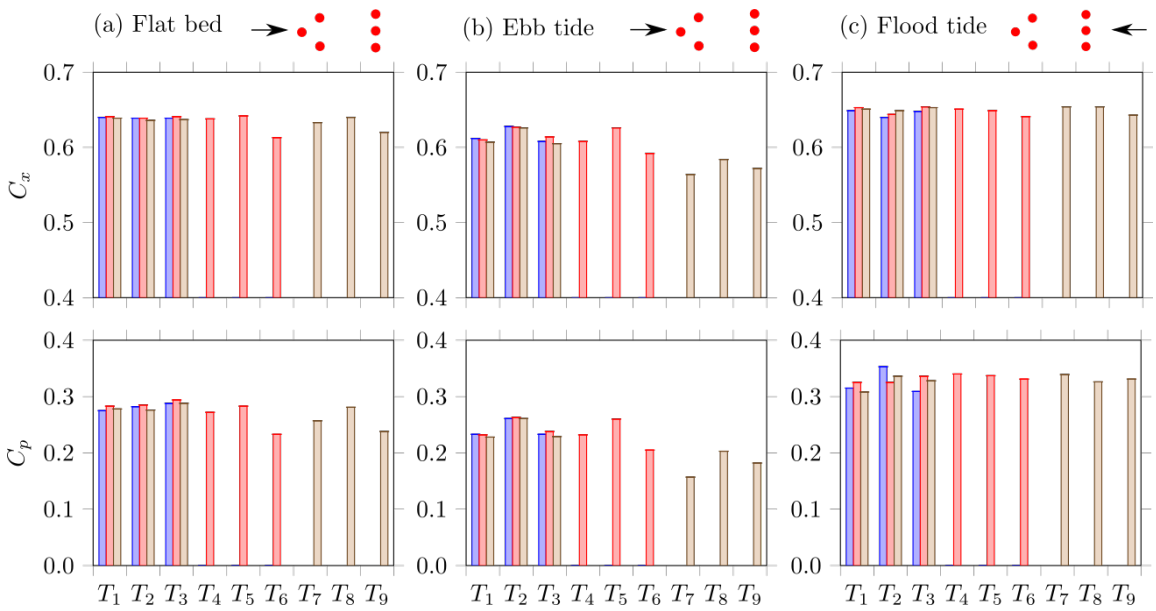

Fig. 8. Thrust and power coefficients obtained for the three arrays simulated, namely: single row array (blue bars), and two-row arrays with a row spacing of $X_s = 12D$ (red bars) and $X_s = 20D$ (yellow bars), for the flat bed case and those with bathymetry during ebb and flodd tides.

[7] J. Slingsby, B. E. Scott, L. Kregting, J. , McIlvenny, J. Wilson, A. Couto, D. Roos, M. Yanez, and B. J. Williamson, "Surface Characterisation of Kolk-Boils within Tidal Stream Environments Using UAV Imagery," *J. Mar. Sci. Eng.*, vol. 9, p. 484, 2021.

[8] M. Sánchez, R. Carballo, V. Ramos, and G. Iglesias, "Tidal stream energy impact on the transient and residual flow in an estuary: A 3D analysis," *Applied Energy*, vol. 116, pp. 167–177, 2014.

[9] N. N, Michelet, N. Guillou, G. Chapalain, J. Thiébot, S. Guillou, A. J. Goward Brown, and S. P. Neill, "Three-dimensional modelling of turbine wake interactions at a tidal stream energy site," *Applied Ocean Research*, vol. 95, p. 102009, 2020.

[10] P. Stansby, "Limitations of depth-averaged modelling of shallow wakes," *ASCE J. Hydraulic Engineering*, vol. 132, pp. 737–740, 2006.

[11] P. Stansby, N. Chini, and P. Lloyd, "Oscillatory flows around a headland by 3D modelling with hydrostatic pressure and implicit bed shear stress comparing with experiment and depth-averaged modelling," *Coastal Engineering*, vol. 116, pp. 1–14, 2016.

[12] D. Culley, S. Funke, S. Kramer, and M. Piggott, "Integration of cost modelling within the micro-siting design optimisation of tidal turbine arrays," *Renewable Energy*, vol. 85, pp. 215–227, 2016.

[13] A. Macleod, S. Porteous, T. Wills, D. Quartel, and A. Watson, "Tidal resource, turbine wake and performance modelling on the EnFAIT project," 2019.

[14] A. C. Bourgoin, S. S. Guillou, J. Thiébot, and R. Ata, "Turbulence characterization at a tidal energy site using large-eddy simulations: Case of the Alderney Race: Alderney Race turbulence les modelling," *Philosophical Transactions of the Royal Society A: Mathematical, Physical and Engineering Sciences*, vol. 378, p. 20190499, 2020.

[15] M. De Dominicis, R. O'Hara Murray, and J. Wolf, "Multi-scale ocean response to a large tidal stream turbine array," *Renewable Energy*, vol. 114, pp. 1160–1179, 2017.

[16] A. Vazquez and G. Iglesias, "A holistic method for selecting tidal stream energy hotspots under technical, economic and functional constraints," *Energy Conversion and Management*, vol. 117, pp. 420–430, 2016.

[17] I. Afgan, J. McNaughton, S. Rolfo, D. D. Apsley, T. Stallard, and P. Stansby, "Turbulent flow and loading on a tidal stream turbine by LES and RANS," *International Journal of Heat and Fluid Flow*, vol. 43, pp. 96–108, 2013.

[18] D. D. Apsley, T. Stallard, and P. K. Stansby, "Actuator-line CFD modelling of tidal-stream turbines in arrays," *Journal of Ocean Engineering and Marine Energy*, vol. 4, pp. 259–271, 2018.

[19] S. Chawdhary, D. Angelidis, J. Colby, D. Corren, L. Shen, and F. Sotiropoulos, "Multiresolution Large-Eddy Simulation of an Array of Hydrokinetic Turbines in a Field-Scale River: The Roosevelt Island Tidal Energy Project in New York City," *Water Resources Research*, vol. 54, pp. 10 188–10 204, 2018.

[20] U. Ahmed, D. D. Apsley, I. Afgan, T. Stallard, and P. K. Stansby, "Fluctuating loads on a tidal turbine due to velocity shear and turbulence: Comparison of CFD with field data," *Renewable Energy*, vol. 112, pp. 235–246, 2017.

[21] G. T. Scarlett, B. Sellar, T. van den Bremer, and I. M. Viola, "Unsteady hydrodynamics of a full-scale tidal turbine operating in large wave conditions," *Renewable Energy*, vol. 143, pp. 199–213, 2019.

[22] P. Ouro, L. Ramírez, and M. Harrold, "Analysis of array spacing on tidal stream turbine farm performance using Large-Eddy Simulation," *Journal of Fluids and Structures*, vol. 91, p. 102732, 2019.

[23] S. Bomminayuni and T. Stoesser, "Turbulence Statistics in an Open-Channel Flow over a Rough Bed," *Journal of Hydraulic Engineering*, vol. 137, pp. 1347–1358, 2011.

[24] T. Stoesser, C. Braun, M. Garcia-Villalba, and W. Rodi, "Turbulence structures in flow over two-dimensional dunes," *Journal of Hydraulic Engineering*, vol. 134, pp. 42–55, 2008.

[25] P. Ouro, U. Lopez-Novoa, and M. F. Guest, "On the performance of a highly-scalable Computational Fluid Dynamics code on AMD, ARM and Intel processor-based HPC systems," *Computer Physics Communications*, vol. 269, p. 108105, 2021.

[26] P. Ouro, B. n. Fraga, U. Lopez-Novoa, and T. Stoesser, "Scalability of an Eulerian-Lagrangian large-eddy simulation solver with hybrid MPI/OpenMP parallelisation," *Computers & Fluids*, vol. 179, pp. 123–136, 2019.

[27] M. Cevheri, R. McSherry, and T. Stoesser, "A local mesh refinement approach for large-eddy simulations of turbulent flows," *International Journal for Numerical Methods in Fluids*, vol. 82, pp. 162–285, 2016.

[28] T. Stoesser, "Large-eddy simulation in hydraulics: Quo Vadis?" *Journal of Hydraulic Research*, vol. 52, pp. 441–452, 2014.

[29] F. Nicoud and F. Ducros, "Subgrid-scale stress modelling based on the square of the velocity," *Flow Measurement and Instrumentation*, vol. 62, pp. 183–200, 1999.

[30] P. Ouro and T. Nishino, "Performance and wake characteristics of tidal turbines in an infinitely large array," *Journal of Fluid Mechanics*, vol. 925, pp. 1–32, 2021.

[31] P. Ouro and T. Stoesser, "Impact of Environmental Turbulence on the Performance and Loadings of a Tidal Stream Turbine," *Flow, Turbulence and Combustion*, vol. 102, pp. 613–639, 2019.

[32] P. Ouro, H. Mullings, and T. Stallard, "Establishing confidence in predictions of fatigue loading for floating tidal turbines based on large-eddy simulations and unsteady blade element momentum," 2022, pp. 915–924.

[33] T. Stallard, T. Feng, and P. K. Stansby, "Experimental study of the mean wake of a tidal stream rotor in a shallow turbulent flow," *Journal of Fluids and Structures*, vol. 54, pp. 235–246, 2015.

[34] P. Stansby and T. Stallard, "Fast optimisation of tidal stream turbine positions for power generation in small arrays with low blockage based on superposition of self-similar far-wake velocity deficit profiles," *Renewable Energy*, vol. 92, pp. 366–375, 2016.
[35] S. Shamsoddin and F. Porté-Agel, "Wind turbine wakes over hills," *Journal of Fluid Mechanics*, vol. 855, pp. 671–702, 2018.